

INVESTIGATION OF SUBGRID-SCALE TURBULENT KINETIC ENERGY IN CHANNEL FLOWS

Kazuhiro Inagaki

Research and Education Center for Natural Sciences
Keio University
4-1-1 Hiyoshi, Kohoku-ku, Yokohama 223-8521, Japan
email: inagakik@keio.jp

Hiromichi Kobayashi

Department of Physics & Research and Education Center for Natural Sciences, Hiyoshi Campus
Keio University
4-1-1 Hiyoshi, Kohoku-ku, Yokohama 223-8521, Japan
email: hkobayas@keio.jp

ABSTRACT

We investigate the subgrid-scale (SGS) turbulent kinetic energy (hereafter referred to as SGS energy) and its transport equation by employing the stabilized mixed model (SMM) developed by Abe (2013). The prediction of the budget for the modeled transport equation is qualitatively well compared with the filtered DNS via the Gaussian filter. In addition, the production term balances with the dissipation rate in the outer region, which suggests that the transport equation can be reduced by assuming the equilibrium between them. We investigate five algebraic expressions for the SGS energy. Among them, the equilibrium form with a newly introduced damping function yields the best compared with the SMM. The zero-equation SMM (ZE-SMM) that employs the equilibrium form instead of the transport equation for the SGS energy provides quantitatively equivalent results as the original SMM. This study paves the way for constructing a convenient anisotropic SGS model that is robust even in coarse grid resolutions.

ANISOTROPIC STRESS MODELING AND SGS ENERGY TRANSPORT

In the recent development of SGS modeling, several studies demonstrated that the anisotropic stress term significantly improves the grid sensitivity of large-eddy simulation (LES) (Abe, 2013; Inagaki & Abe, 2017; Marstorp *et al.*, 2009; Montecchia *et al.*, 2017). Abe (2019) and Inagaki & Kobayashi (2020) revealed that the anisotropic stress term essentially contributes to the generation of the grid-scale (GS) or resolved-scale Reynolds shear stress and energy spectrum at the high-wavenumber region. Therefore, the investigation of the anisotropic SGS stress models paves the way for the further development of LES of a more high-Reynolds number turbulent flows.

In these anisotropic models, the SGS energy is employed in the transport coefficients of the modeled stress. Especially in the SMM (Abe, 2013), the SGS energy is obtained by numerically solving its transport equation, which is referred to as the one-equation model (OEM). In the OEM with the eddy-viscosity assumption, the balance between the produc-

tion and dissipation terms in the SGS energy transport yields the Smagorinsky model (Smagorinsky, 1963). Therefore, we can interpret that the OEM incorporates the nonequilibrium effect on the transport coefficients. One may consider that the nonequilibrium effect resulting from the OEM significantly contributes to the robustness of the SMM against the grid resolution. However, the physical nature of OEMs has not been investigated in detail yet. In general, solving an additional transport equation can be a numerical burden and lose the convenience of the model. Furthermore, the modeled transport equation does not guarantee the positive semi-definiteness of the SGS energy. Consequently, the negative SGS energy must be clipped when the eddy viscosity is modeled in terms of its square root. If the OEM is reduced to an algebraic or zero-equation model of SGS energy in a physically reliable manner, the convenience of the SGS model significantly increases.

In the present study, we investigate the physical property of the OEM via the SMM with the filtered DNS data in turbulent channel flows. Thanks to the robustness of the SMM against the grid resolution, we can investigate the SGS energy in a coarse grid resolution in which the SGS energy is healthier than the conventional LES with the eddy-viscosity models. We also demonstrate the reduction of the SMM into the ZE-SMM that excludes the transport equation for the SGS energy.

Introduction of SMM and OEM

In the SMM, the SGS stress $\tau_{ij}^{\text{sgs}} (= \overline{u_i u_j} - \bar{u}_i \bar{u}_j)$ is modeled as follows:

$$\tau_{ij}^{\text{sgs}} = \frac{2}{3} k^{\text{sgs}} \delta_{ij} - 2\nu^{\text{sgs}} \bar{s}_{ij} + \tau_{ij}^{\text{eat}}, \quad \tau_{ij}^{\text{eat}} = 2k^{\text{sgs}} \frac{\tau_{ij}^{\text{a}}|_{\text{t}} + 2\nu^{\text{a}} \bar{s}_{ij}}{\tau_{\ell\ell}^{\text{a}}},$$

$$\nu^{\text{a}} = -\frac{\tau_{ij}^{\text{a}}|_{\text{t}} \bar{s}_{ij}}{2\bar{s}_{\ell m} \bar{s}_{\ell m}}, \quad \tau_{ij}^{\text{a}} = (\bar{u}_i - \hat{u}_i)(\bar{u}_j - \hat{u}_j). \quad (1)$$

Here, $k^{\text{sgs}} (= \tau_{\ell\ell}^{\text{sgs}}/2)$ and ν^{sgs} denote the SGS energy and eddy viscosity, respectively. $\bar{\cdot}$ and $\hat{\cdot}$ denote the filter and test filter operations, respectively. u_i is the velocity field and $\bar{s}_{ij} [= (\partial \bar{u}_i / \partial x_j + \partial \bar{u}_j / \partial x_i) / 2]$ is the GS strain rate. The SGS

eddy viscosity ν^{sgs} is expressed by

$$\nu^{\text{sgs}} = C_{\text{sgs}} f_v \bar{\Delta} \sqrt{k^{\text{sgs}}}, \quad f_v = 1 - \exp[-(d_\varepsilon/A_0)^{2/(1+C_0)}],$$

$$d_\varepsilon = \frac{u_\varepsilon y}{\nu} \left(\frac{y}{\bar{\Delta}} \right)^{C_0}, \quad u_\varepsilon = (\nu \varepsilon^{\text{sgs}})^{1/4}. \quad (2)$$

Here, $\bar{\Delta}$ denotes the filter length scale and ν is the kinematic viscosity. ε^{sgs} will be provided later. Inagaki & Abe (2017) suggested the following parameters: $\bar{\Delta} = (\Delta x \Delta y \Delta z)^{1/3}$, $C_{\text{sgs}} = 0.075$, $A_0 = 13$, and $C_0 = 1/3$. Δx , Δy , and Δz are the grid spacing in each direction in a Cartesian coordinate. The filter length scale for the test filter is set to be $\hat{\Delta} = 2\bar{\Delta}$.

In OEMs including the SMM, k^{sgs} is obtained by numerically solving the following transport equation:

$$\frac{\partial k^{\text{sgs}}}{\partial t} = -\frac{\partial}{\partial x_i} (\bar{u}_i k^{\text{sgs}}) - \tau_{ij}^{\text{sgs}} \bar{s}_{ij} - \varepsilon^{\text{sgs}}$$

$$- \frac{\partial}{\partial x_j} (T_j^{\text{t,sgs}} + T_j^{\text{p,sgs}}) + \nu \frac{\partial^2 k^{\text{sgs}}}{\partial x_i \partial x_i}, \quad (3)$$

where $\varepsilon^{\text{sgs}} = \nu [(\partial \bar{u}_i / \partial x_j)^2 - (\partial \bar{u}_i / \partial x_j)^2]$, $T_j^{\text{t,sgs}} = \bar{u}_j \bar{u}_i \bar{u}_i / 2 - \bar{u}_j \bar{u}_i \bar{u}_i / 2 - \bar{u}_i \tau_{ij}^{\text{sgs}}$, and $T_j^{\text{p,sgs}} = \bar{p} \bar{u}_j - \bar{p} \bar{u}_j$. We refer to the terms on the right-hand side of Eq. (3) as convection, production, dissipation, turbulent diffusion, pressure diffusion, and viscous diffusion, respectively. In OEMs, ε^{sgs} and $T_j^{\text{t,sgs}} + T_j^{\text{p,sgs}}$ are modeled as follows:

$$\varepsilon^{\text{sgs}} = C_\varepsilon \frac{(k^{\text{sgs}})^{3/2}}{\bar{\Delta}} + \frac{2\nu k^{\text{sgs}}}{y^2}, \quad (4)$$

$$T_j^{\text{t,sgs}} + T_j^{\text{p,sgs}} = -C_k f_v \bar{\Delta} \sqrt{k^{\text{sgs}}} \frac{\partial k^{\text{sgs}}}{\partial x_j}. \quad (5)$$

Here, y denotes the distance from the solid wall. The second term on the right-hand side of Eq. (4) is the wall correction term. We set $C_\varepsilon = 0.835$ and $C_k = 0.1$ (Inagaki & Abe, 2017). Note that in the SMM, $\tau_{ij}^{\text{at}} \bar{s}_{ij} = 0$ owing to the stabilization treatment of the ν^{a} -related term. Hence, the production always yields a positive. Namely, $-\tau_{ij}^{\text{sgs}} \bar{s}_{ij} = 2\nu^{\text{sgs}} \bar{s}^2 \geq 0$ where $\bar{s}^2 = \bar{s}_{ij} \bar{s}_{ij}$.

NUMERICAL SIMULATION

We perform LESs of the SMM and DNS in turbulent channel flows in a Cartesian coordinate with a staggered grid system. x , y , and z denote the streamwise, wall-normal, and spanwise directions, respectively. For details of the numerical schemes, please refer to Inagaki & Kobayashi (2020, 2022). For the reference LES of the eddy-viscosity model, we also perform the case with $\tau_{ij}^{\text{at}} = 0$ and $C_{\text{sgs}} = 0.042$ in the SMM, which is referred to as the EVM. Note that $C_{\text{sgs}} = 0.042$ is the best value for the eddy-viscosity-based OEMs (Inagaki, 2011; Inagaki & Kobayashi, 2020). The Reynolds number is set to be $\text{Re}_\tau (= u_\tau h / \nu) = 400$ where h , $u_\tau (= \sqrt{|\partial U_x / \partial y|_{\text{wall}}|})$, and $U_x (= \langle \bar{u}_x \rangle)$ denote the channel half width, wall-friction velocity, and mean velocity, respectively. For the LES at higher Reynolds numbers, we also perform the cases at $\text{Re}_\tau = 1000$ and 2000. The statistical average $\langle \cdot \rangle$ is taken over the x - z plane and time. Details of the parameters are provided in Table 1. Here and hereafter, the values with the superscript “+” indicate those normalized by ν and u_τ . For the analysis of the

Table 1. Numerical parameters. The domain size is $L_x \times L_y \times L_z = 2\pi h \times 2h \times \pi h$. LR and MR denote the low and medium resolutions, respectively.

Case	Re_τ	$N_x \times N_y \times N_z$	Δx^+	Δz^+
SMM LR	400	$24 \times 64 \times 16$	105	79
SMM MR	400	$48 \times 64 \times 32$	52	39
EVM LR	400	$24 \times 64 \times 16$	105	79
EVM MR	400	$48 \times 64 \times 32$	52	39
DNS	400	$256 \times 192 \times 256$	9.8	4.9
SMM1000	1000	$48 \times 96 \times 32$	131	98
SMM2000	2000	$96 \times 128 \times 64$	131	98

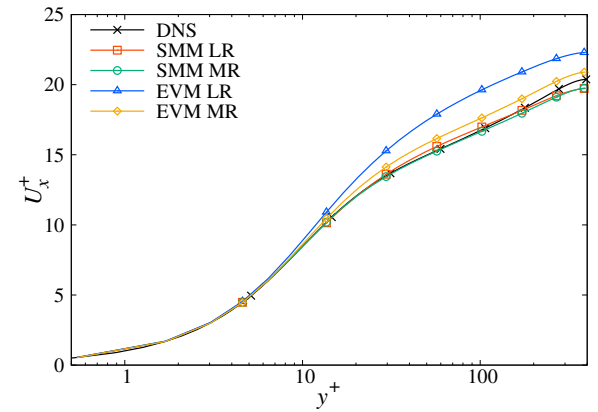


Figure 1. Mean velocity profiles for the DNS, SMM, and EVM at $\text{Re}_\tau = 400$ in each grid resolution.

filtered DNS, we employ the Gaussian filter only in the x and z directions where the cut-off wavenumber corresponds to the maximum wavenumber of the LES.

Numerical results

Figure 1 shows the mean velocity profiles for the DNS, SMM, and EVM at $\text{Re}_\tau = 400$. The EVM overestimates the mean velocity in the LR. In contrast, for the SMM, the mean velocity profiles are comparable to the DNS for both resolutions. Figure 2 shows the budgets for the SGS energy transport equation for the filtered DNS and SMM in the LR. Although the SMM overestimates the production and dissipation rates in the near-wall region, the prediction of the SMM is fairly well compared with the filtered DNS. Furthermore, the production term balances with the dissipation rate in $y^+ > 50$, which suggests that the transport equation can be reduced by assuming the production-dissipation equilibrium.

Figure 3 shows the correlation between the production and dissipation terms in the SGS energy transport equation, where the correlation coefficient is defined by $\text{cor}(f, g) = \langle f'g' \rangle / \sqrt{\langle f'^2 \rangle \langle g'^2 \rangle}$ with $f' = f - \langle f \rangle$. For the filtered DNS, the correlation is low. Hence, the local equilibrium assumption is poor, as it is classically discussed. This result is obvious because the backscatters often occur in the filtered DNS, which must not balance with the local dissipation. In contrast, the LESs of both the SMM and EVM provide a high correlation

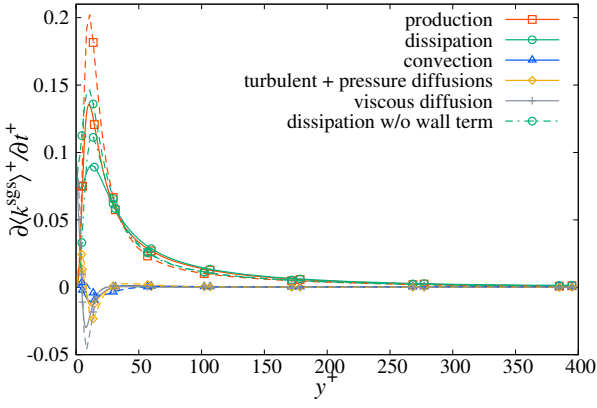


Figure 2. Budgets for the SGS energy transport equation for the DNS (solid lines with symbols) and SMM (dashed lines with symbols) at $Re_\tau = 400$ in the LR. The dash-dotted line represents the dissipation term without wall correction in the SMM; $\langle C_\epsilon (k^{sgs})^{3/2} / \Delta \rangle$.

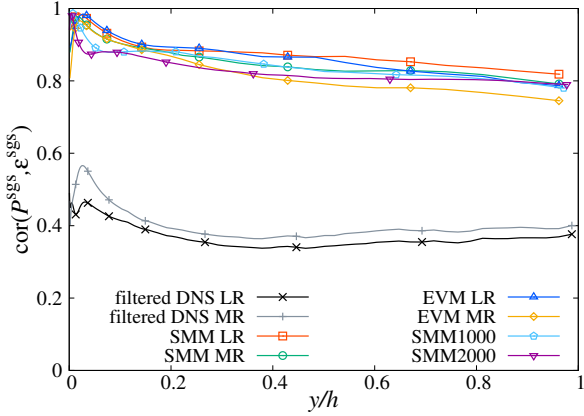


Figure 3. Correlation coefficient between the production P^{sgs} and dissipation ϵ^{sgs} for the filtered DNS, SMM and EVM. Note that for the LESs, the dissipation term excludes the wall correction term; namely, $\epsilon^{sgs} = C_\epsilon (k^{sgs})^{3/2} / \Delta$ is employed.

that yields 80%. In addition, the correlation is high at high-Reynolds-number cases. This result partly emanates from the modeling of the production term given by $2\nu^{sgs}\bar{s}^2$, which is always positive and excludes the backscatter. Therefore, if the OEMs employ the eddy-viscosity-based production term, the local production–dissipation equilibrium assumption can be a good model.

Reduction of SMM employing an algebraic expression for SGS energy

In the region away from the wall, the local production–dissipation equilibrium in the SGS energy transport equation yields $k^{sgs} = (2C_{sgs}/C_\epsilon)\bar{\Delta}^2\bar{s}^2$. However, this model cannot be applied in the near-wall region because \bar{s}^2 does not decrease, whereas k^{sgs} must decrease as $O(y^2)$. A primitive approach to representing the proper near-wall behavior is to employ a damping function. A basic damping function is $1 - \exp[-(y^+/A)^2]$ with a constant A . However, the wall-friction velocity u_τ is not always a suitable variable for the damping function because it yields zero at a separation point (see e.g. Inagaki, 2011). Here, we introduce a new damping function that is applicable to the turbulent flows with separa-

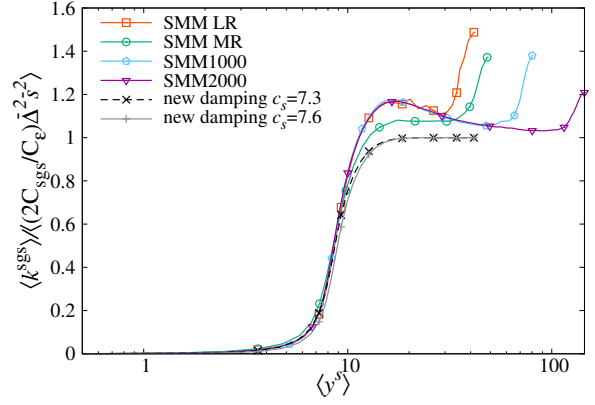


Figure 4. Ration of the SGS energy to the local equilibrium expression for the SMM with respect to the mean distance from the wall normalized by the GS Kolmogorov length scale $\langle y^s \rangle$.

tion points:

$$f_k = \frac{1 - \exp[-(y^s/a_s)^2]}{1 + \exp[-b_s y^s + c_s]}, \quad y^s = \frac{y(\bar{s}^2)^{1/4}}{\nu^{1/2}}. \quad (6)$$

Here, y^s can be interpreted as the distance from the wall normalized by the GS Kolmogorov length scale. Namely, $y^s = y/\eta^{sgs}$ with $\eta^{sgs} = (\nu\epsilon^{sgs}/2)^{1/4}$ and $\epsilon^{sgs} = 2\nu\bar{s}^2$. The numerator of f_k realizes the near-wall asymptote $f_k \sim O(y^2)$, whereas the denominator represents the strong damping of the SGS energy in the vicinity of the wall.

Figure 4 shows the profiles of the ratio of the SGS energy to the local equilibrium expression for the SMM with respect to the mean distance from the wall normalized by the GS Kolmogorov length scale $\langle y^s \rangle$. This ratio corresponds to the exact damping behavior in the near-wall region. Note that $y^+ = 50$ and 100 correspond to $\langle y^s \rangle = 10$ and 20, respectively. Regardless of the Reynolds number, the ratio almost collapses to a single curve in the near-wall region. The black dashed line with crosses depicts the best fit curve obtained by minimizing the mean square error of the SGS energy between the exact profile and model expression for the SMM at $Re_\tau = 400$ in the LR. The parameters yield $a_s = 0.6$, $b_s = 0.77$, and $c_s = 7.3$. However, in the *a posteriori* test that employs the algebraic expression of SGS energy with this damping function, the mean velocity is slightly underestimated with these parameters. Therefore, in the *a posteriori* test, we refine the parameter as $c_s = 7.6$. The damping function with the refined parameter is plotted in Fig. 4 in the gray solid line with pluses.

In LES, we can employ the scale-similarity models (Bardina *et al.*, 1983) as a representative quantity to express the model of SGS energy. The dynamic procedure (Marstorp *et al.*, 2009; Montecchia *et al.*, 2017) or invariants of the velocity gradient (Kobayashi, 2005; Silvis *et al.*, 2017) are also useful in expressing the near-wall asymptote of the SGS energy. Here, we compare the following algebraic expressions for the SGS energy calculated in the SMM with the result via the transport equation:

1. SGS-Reynolds form

$$C_S(\bar{u}_i - \hat{u}_i)(\bar{u}_i - \hat{u}_i), \quad (7)$$

2. dynamic form (Marstorp *et al.*, 2009; Montecchia *et al.*, 2017)

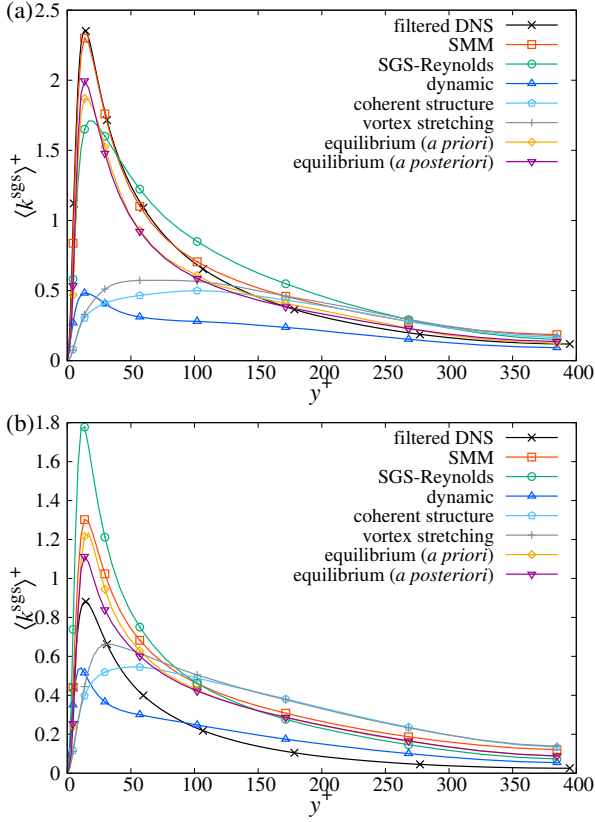


Figure 5. Profiles of the SGS energy for the filtered DNS, SMM, and several model expressions calculated in the SMM in (a) LR and (b) MR at $Re_\tau = 400$.

$$2C_D \bar{\Delta}^{-2} \bar{s}^2, \quad C_D = \frac{1}{4} \frac{\langle LM \rangle}{\langle M^2 \rangle},$$

$$L = \widehat{\bar{u}_i \bar{u}_i} - \widehat{\bar{u}_i} \widehat{\bar{u}_i}, \quad M = \frac{\Delta^2}{\bar{\Delta}^2} \bar{s}^2 - \bar{\Delta}^{-2} \widehat{\bar{s}^2}, \quad (8)$$

3. coherent structure form (Kobayashi, 2005)

$$C_{CS} F_{CS} \bar{\Delta}^{-2} \bar{s}^2, \quad F_{CS} = \frac{|\bar{w}^2 - \bar{s}^2|}{\bar{w}^2 + \bar{s}^2}, \quad (9)$$

4. vortex stretching form (Silvis *et al.*, 2017)

$$C_{VS} F_{VS} \bar{\Delta}^{-2} \bar{s}^2, \quad F_{VS} = \frac{(\bar{s}_{ij} \bar{\omega}_j)^2}{\bar{s}^2 \bar{\omega}_\ell^2}, \quad (10)$$

5. equilibrium form with the new damping function

$$f_k \frac{2C_{sgs}}{C_\epsilon} \bar{\Delta}^{-2} \bar{s}^2, \quad (11)$$

where $\bar{w}_{ij} = (\partial \bar{u}_i / \partial x_j - \partial \bar{u}_j / \partial x_i) / 2$, $\bar{\omega}_i = \epsilon_{ij\ell} \partial \bar{u}_\ell / \partial x_j$, and f_k is provided by Eq. (6) with $a_s = 0.6$, $b_s = 0.77$, and $c_s = 7.6$. All model expressions satisfy the near-wall asymptote $k^{sgs} \sim O(y^2)$. The model constants are set to be $C_S = 2.5$, $C_{CS} = 0.7$, and $C_{VS} = 1.1$.

Figures 5(a) and (b) show the profiles of the SGS energy for the filtered DNS, SMM, and several model expressions calculated in the SMM provided by Eqs. (7)–(11) in the LR and MR, respectively, at $Re_\tau = 400$. In the LR, the profile of the SMM is reasonable compared with the filtered DNS. However, in the MR, the SMM overestimates the SGS energy compared with the filtered DNS. Hence, we can observe that the OEM

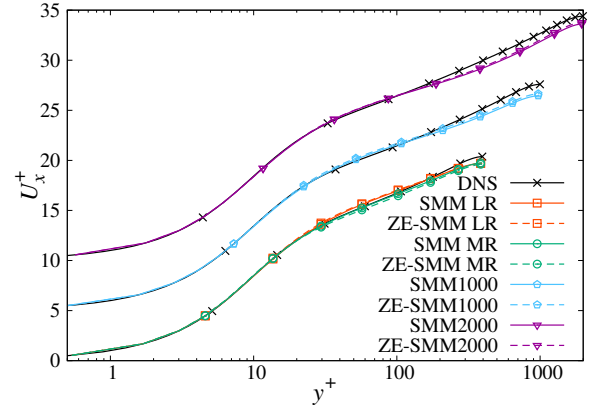


Figure 6. Mean velocity profiles for the DNS, SMM, and ZE-SMM. The results for $Re_\tau = 1000$ and 2000 are shifted by a factor of five and ten, respectively. The DNSs at $Re_\tau = 1000$ and 2000 are performed by Lee & Moser (2015).

with the SMM does not necessarily predict the profile of the SGS energy for the filtered DNS. Although the SGS-Reynolds form seems to be reasonable in the LR, it excessively overestimates the profile. Hence, if we employ the SGS-Reynolds form instead of the OEM, the model will highly depend on the grid resolution. The dynamic, coherent structure, and vortex stretching forms fail to reproduce the sharp profile in the near-wall region. In contrast, the equilibrium form succeeds in predicting the sharp profiles like the filtered DNS and SMM. For the equilibrium form, we also plot the result of the *a posteriori* test, which is almost similar to that of the *a priori* test. Note that the *a priori* test indicates the prediction using the data of the SMM, whereas the *a posteriori* test indicates the result of the simulation of the ZE-SMM that employs the equilibrium model for the SGS energy instead of solving its transport equation. Among five model expressions (7)–(11), the equilibrium form with the new damping function yields the best compared with the SMM. Therefore, we expect that the equilibrium form with the new damping function (11) can provide a similar result compared with the original OEM-based SMM.

Performance of ZE-SMM

Figure 6 shows the mean velocity profiles for the DNS, SMM, and ZE-SMM. For all cases, the ZE-SMM provides a comparable profile compared with the original OEM-based SMM and well predicts the profile of the DNS. The total turbulent kinetic energy K is defined as

$$K = \frac{1}{2} \langle \bar{u}_i \bar{u}_i \rangle + \langle k^{sgs} \rangle. \quad (12)$$

This decomposition is unique when the filtering is employed only in the directions that the spatial average is taken. In the present LESs, we assume that the right-hand side of Eq. (12) yields the total turbulent kinetic energy despite the employment of an implicit filtering operation in the y direction. Figure 7 shows the profiles of the total turbulent kinetic energy for the DNS, SMM, and ZE-SMM. The ZE-SMM provides almost the same profile as the original SMM for all cases, although the SGS energy decreases as seen in Fig. 5. For high-Reynolds-number cases of $Re_\tau = 1000$ and 2000 , both the SMM and ZE-SMM slightly underestimate the total turbulent kinetic energy in the outer region. Further improvement of the SGS model

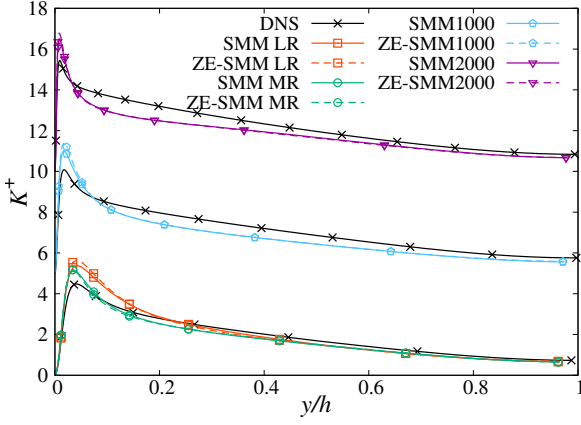


Figure 7. Profiles of the total turbulent kinetic energy for the DNS, SMM, and ZE-SMM. The results for $Re_\tau = 1000$ and 2000 are shifted by a factor of five and ten, respectively. The DNSs at $Re_\tau = 1000$ and 2000 are performed by Lee & Moser (2015).

is required to reproduce a more accurate profile of the total turbulent kinetic energy.

Inagaki & Kobayashi (2020) suggested that the enhancement of small-scale turbulence contributes to the robustness of the SMM against the grid resolution. The GS Reynolds stress spectrum is defined by

$$E_{ij}^{GS}(k_x, y) = \Re \langle \tilde{u}_i \tilde{u}_j^* \rangle, \quad (13)$$

where we consider the Fourier transformation only in the x direction:

$$\tilde{u}_i(k_x, y, z) = \frac{1}{L_x} \int_0^{L_x} dx \bar{u}_i(x, y, z) \exp[-ik_x x]. \quad (14)$$

We focus on the most energetic part, that is, the streamwise component E_{xx}^{GS} . Figure 8 shows the streamwise component of the premultiplied GS Reynolds stress spectrum for the filtered DNS, SMM, ZE-SMM, and EVM. Here, the $\lambda_x (= 2\pi/k_x)$ is the wavelength. The filtered DNS provides a large intensity of the spectrum even in the small scales $\lambda_x^+ < 300$. The result of the ZE-SMM is almost the same as that of the SMM, which indicates that the reduction of the OEM by employing the algebraic model (11) does not change the statistical property of the SMM. Both the SMM and ZE-SMM also provide a large intensity in the small scales $\lambda_x^+ < 300$ in the near-wall region $y^+ < 50$. In the outer region, the SMM and ZE-SMM provide a smaller intensity than the filtered DNS. To predict the large intensity in the outer region, we have to further improve the SGS model. For the EVM, the spectrum rapidly decreases in the small scale $\lambda_x^+ < 400$. This underestimation of the spectrum results from the poor physical role of the eddy-viscosity models (see Inagaki & Kobayashi, 2020). The anisotropic stress is essential in the reproduction of small-scale turbulence.

CONCLUSIONS

We investigated the transport equation for the SGS energy in turbulent channel flows via the DNS and LES employing the SMM. Thanks to the robustness of the SMM against the grid resolution, we succeeded in examining the properties of the

SGS energy and its transport under the condition that the SGS energy is healthier than the conventional LESs. For the LR case at $Re_\tau = 400$, the peak value of the SGS energy is approximately 50% of that of the total turbulent kinetic energy (see Figs. 5 and 7) even though the mean velocity profile is comparable to the DNS. The budget of the modeled transport equation for the SGS energy is qualitatively comparable with the exact one calculated in the filtered DNS. In the budget, the production term balances with the dissipation rate in the outer region. For the filtered DNS, as is well known, the correlation between the production and dissipation terms is low. In contrast, for the LESs employing the OEM, the production term correlates well with the dissipation. This result indicates that the local production–dissipation equilibrium assumption can be a good approximation for the OEMs, although this assumption does not hold in the filtered DNS.

To construct an algebraic expression for the SGS energy based on the local equilibrium assumption, we introduced a new damping function where the distance from the solid wall is normalized by the GS Kolmogorov length scale. The ratio of the SGS energy to the local equilibrium model almost collapses to a single curve when it is plotted with respect to the mean distance from the solid wall normalized by the GS Kolmogorov length scale. Based on this curve, we developed a new damping function. We compared the profiles of the SGS energy for the filtered DNS, SMM, and several model expressions including the local equilibrium model with the damping function. Among the model expressions provided in the present analysis, the equilibrium model with the damping function yields the best prediction compared with the result of the transport equation in the SMM.

Finally, we performed the reduced model of the SMM that employs the equilibrium form with the damping function for the SGS energy instead of solving the transport equation, which is referred to as the ZE-SMM. The ZE-SMM has the equivalent performance compared with the original OEM-based SMM. Namely, the ZE-SMM provides quantitatively similar results to the SMM for the profiles for the mean velocity, total turbulent kinetic energy, and streamwise component of the GS Reynolds stress spectrum. Consequently, the present study revealed that the conventional SGS energy transport equation is not essential in realizing the preferable properties of the SMM. Although the investigation has been conducted only in turbulent channel flows, the present reduction from the OEM to the equilibrium model is expected to be valid in other turbulent flows (for details, see Inagaki & Kobayashi, 2022).

The success of the reduction using the local equilibrium assumption partly results from the modeling of the production term expressed in terms of the eddy viscosity and strain rate, which does not provide the backscatter. There is the possibility that the OEM that allows the backscatter improves the SGS models. However, in the OEMs, the SGS energy must be positive because its square root is usually employed in the eddy viscosity. The modeling of the SGS energy transport equation that allows both the backscatter and positive semi-definiteness is challenging. The local equilibrium expression is a primitive model for the SGS energy. The present study paves the way for the further development of the SGS modeling that requires the model expression of SGS energy.

ACKNOWLEDGMENTS

K.I. was supported by a Grant-in-Aid for JSPS Fellows Grant No. JP21J00580.

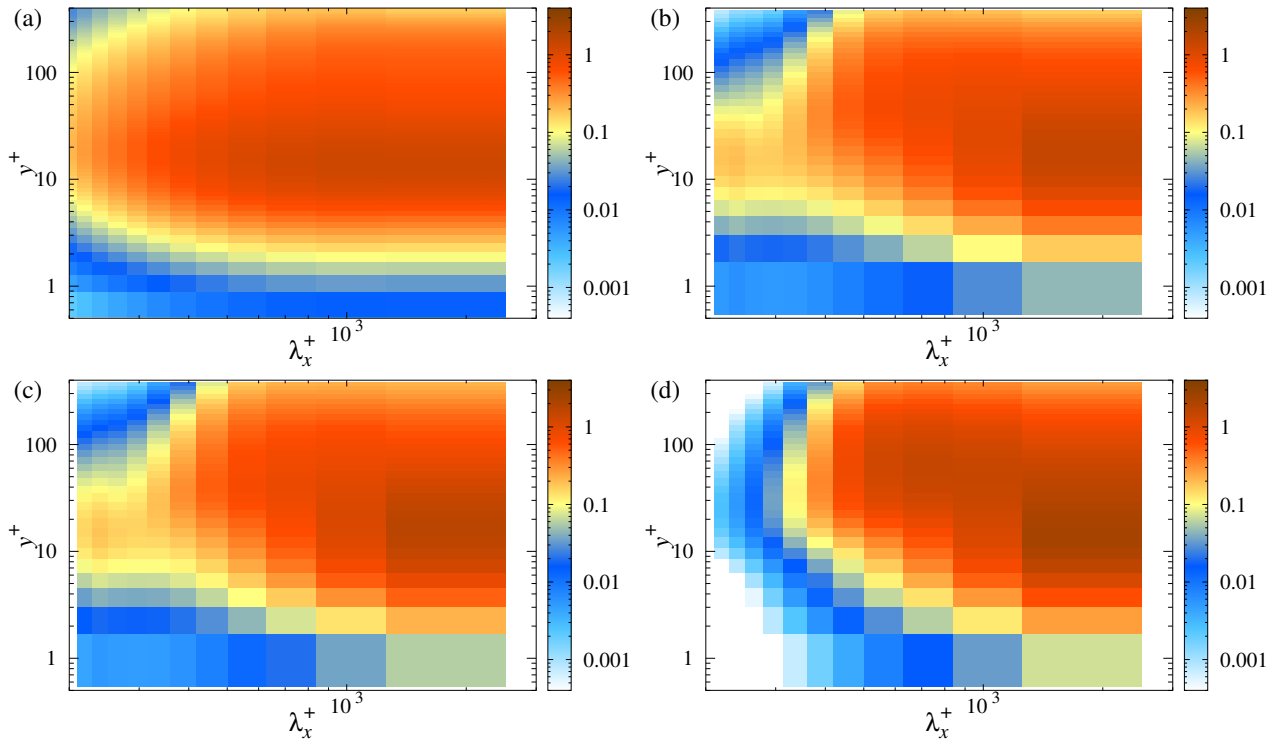


Figure 8. Contour maps of the streamwise component of the premultiplied GS Reynolds stress spectrum $k_x E_{xx}^{GS}$ for (a) filtered DNS (b) SMM, (c) ZE-SMM, and (d) EVM in the LR at $Re_\tau = 400$.

REFERENCES

- Abe, K. 2013 An improved anisotropy-resolving subgrid-scale model with the aid of a scale-similarity modeling concept. *Int. J. Heat Fluid Flow* **39**, 42–52.
- Abe, K. 2019 Notable effect of the subgrid-scale stress anisotropy on mean-velocity prediction through budget of the grid-scale Reynolds-shear stress. *Phys. Fluids* **31**, 105103.
- Bardina, J., Ferziger, J. H. & Reynolds, W. C. 1983 Improved turbulence models based on large eddy simulation of homogenous, incompressible, turbulent flows. *Report TF-19. Thermosciences Division, Dep. of Mech. Eng., Stanford University, Stanford, California*.
- Inagaki, K. & Kobayashi, H. 2020 Role of various scale-similarity models in stabilized mixed subgrid-scale model. *Phys. Fluids* **32**, 075108.
- Inagaki, K. & Kobayashi, H. 2022 Transport and modeling of subgrid-scale turbulent kinetic energy in channel flows. *AIP Advances* **12**, 045222.
- Inagaki, M. 2011 A new wall-damping function for large eddy simulation employing Kolmogorov velocity scale. *Int. J. Heat Fluid Flow* **32**, 26–40.
- Inagaki, M. & Abe, K. 2017 An improved anisotropy-resolving subgrid-scale model for flows in laminar-turbulent transition region. *Int. J. Heat Fluid Flow* **64**, 137–152.
- Kobayashi, H. 2005 The subgrid-scale models based on coherent structures for rotating homogeneous turbulence and turbulent channel flow. *Phys. Fluids* **17**, 045104.
- Lee, M. & Moser, R. D. 2015 Direct numerical simulation of turbulent channel flow up to $re_\tau \approx 5200$. *J. Fluid Mech.* **774**, 395–415.
- Marstorp, L., Brethouwer, G., Grundestam, O. & Johansson, A. V. 2009 Explicit algebraic subgrid stress models with application to rotating channel flow. *J. Fluid Mech.* **639**, 403–432.
- Montecchia, M., Brethouwer, G., Johansson, A. V. & Wallin, S. 2017 Taking large-eddy simulation of wall-bounded flows to higher Reynolds numbers by use of anisotropy-resolving subgrid models. *Phys. Rev. Fluids* **2**, 034601.
- Silvis, M. H., Remmerswaal, R. A. & Verstappen, R. 2017 Physical consistency of subgrid-scale models for large-eddy simulation of incompressible turbulent flows. *Phys. Fluids* **29**, 015105.
- Smagorinsky, J. 1963 General circulation experiments with the primitive equations. I. The basic experiment. *Mon. Weather Rev.* **91**, 99–164.